J. Nano- Electron. Phys.
3 (2011) No1, P. 1021-1034

PACS numbers: 68.37.Hk, 68.37.Ps

POROUS SILICON & TITANIUM DIOXIDE COATINGS PREPARED BY ATMOSPHERIC PRESSURE PLASMA JET CHEMICAL VAPOUR DEPOSITION TECHNIQUE-A NOVEL COATING TECHNOLOGY FOR PHOTOVOLTAIC MODULES

***S. Bhatt*[1], *J. Pulpytel*[1], *F. Krcma*[2], *V. Mazankova*[2], *F. Arefi-Khonsari*[1]**

[1] Laboratoire de Génie des Procédés Plasmas et Traitements de Surfaces (LGPPTS), Université Pierre et Marie Curie (UPMC), ENSCP, 11, Rue Pierre et Marie Curie, 75231, Paris, Cedex 05, France
E-mail: sudhir_rhyme@yahoo.co.in, jerome-pulpytel@chimie-paristech.fr

[2] Institute of Physical and Applied Chemistry, Faculty of Chemistry, Brno University of Technology, Purkyňova 118, 612 00, Brno, Czech Republic

Atmospheric Pressure Plasma Jet (APPJ) is an alternative for wet processes used to make anti reflection coatings and smooth substrate surface for the PV module. It is also an attractive technique because of it's high growth rate, low power consumption, lower cost and absence of high cost vacuum systems. This work deals with the deposition of silicon oxide from hexamethyldisiloxane (HMDSO) thin films and titanium dioxide from tetraisopropyl ortho titanate using an atmospheric pressure plasma jet (APPJ) system in open air conditions. A sinusoidal high voltage with a frequency between 19-23 *kHz at power up to* 1000 *W was applied between two tubular electrodes separated by a dielectric material. The jet, characterized by* T_g ~ 600-800*K, was mostly laminar (Re* ~ 1200*) at the nozzle exit and became partially turbulent along the jet axis (Re* ~3300*). The spatially resolved emission spectra showed* OH, N_2, N_2^+ *and* CN *molecular bands and* O, H, N, Cu *and* Cr *lines as well as the* NO_2 *chemiluminescence continuum (*450-800 *nm). Thin films with good uniformity on the substrate were obtained at high deposition rate, between* 800-1000 *nm.s*$^{-1}$*, and AFM results revealed that coatings are relatively smooth (Ra* ~ 2 *nm). The FTIR and SEM analyses were better used to monitor the chemical composition and the morphology of the films in function of the different experimental conditions.*

Keywords: *POROUS* SiO_2, *POROUS* TiO_2, *ATMOSPHERIC PRESSURE PLASMA CHEMICAL VAPOUR DEPOSITION (APCVD), HIGH DEPOSITION RATE.*

(Received 04 February 2011, in final form 02 December 2011)

1. INTRODUCTION

Porous Silica (PS) was discovered in 1990 and was formed on crystalline-silicon wafers using electrochemical etching. Such film exhibits photo luminescent and electroluminescent properties similar to those properties of a semiconductor with a direct energy gap [1]. PS layers can be easily produced on single or multicrystalline silicon surfaces by electrochemical or stain etching. Several possible methods of using PS to improve the performance of crystalline silicon solar cells have been proposed since then. It was shown that a PS etched silicon surface has excellent anti-reflection

properties [2]. PS may also serve as a wide band gap absorber in a multiple-junction cell structure, with crystalline silicon as the substrate or as gettering centres to reduce the impurity levels in a silicon substrate [3]. A PS back-surface reflector has been demonstrated for thin-film silicon solar cells [4]. Attempts were even made to use two PS layers with two different band gaps in a three-band gap (Eg) solar cell on a silicon wafer [5].

In recent years, porous silica (SiO_2) films were successfully used as efficient antireflection (AR) coatings on glass and transparent polymer covers of photovoltaic modules because they feature effective refractive indices below 1.5 in the visible and infrared wavelength region [6]. Today, porous SiO_2 AR coatings are commonly prepared by sol gel deposition [7]. However, this technique has a number of demerits: (a) the use of wet chemicals causes wettability problems on substrates like polymers leading to non uniform coatings, (b) elevated temperatures must usually be applied in order to completely evaporate the solvents in the drying step, (c) almost no control on coating thickness can be obtained and hence the refractive index can not be tuned. Other deposition technologies investigated like wet chemical etching of glass substrates [8] and oblique incident thermal evaporation [9] eliminate some of the mentioned disadvantages. But in the wet processes, some of the highly concentrated chemical mixtures which are used are not environmentally friendly. Porous SiO_2 films can be deposited by thermal evaporation [10], sputtering and low pressure chemical vapor deposition [11] and electron beam (EB) evaporation [12]. However, the need for high-vacuum system makes such processes very costly and time consuming.

Photonic devices based on organic materials have attracted much interest and have been competing with the inorganic based devices for potential applications. Among these applications, dye-sensitized solar cells (DSSC) based on porous titanium dioxide (TiO_2) particles and organic dyes have demonstrated energy conversion efficiencies of around 10 %, comparable to amorphous silicon based solar cells [13]. DSSC have possibilities of high energy conversion efficiency and low fabrication cost [14]. DSSC, titanium dioxide (TiO_2) is one of the most promising materials used for porous thin films due to its appropriate energy levels, dye adsorption ability, low cost, and easy preparation [15]. Porous TiO_2 has been deposited by wet, spin coating, dip-coating technique etc [16] for DSSC.

Up to now none of the known deposition technologies for porous SiO_2 AR and porous TiO_2 coatings have proven their superior potential for large-scale industrial production.

In this work an alternative technology for the preparation of porous SiO_2 AR and porous TiO_2 coatings are presented Atmospheric Pressure Plasma Jet Chemical Vapour Deposition system (APCVD). Plasma processes, especially APCVD, seems to be a potential alternative to these wet-chemical processes.This technique is already well established for the surface activation [17]. Different jet sources have been investigated for the deposition of silicon-based coatings such as RF driven jet source [18] or a DC Arc Jet [19] as well as a commercially available open air plasma jet (Plasmatreat, Gmbh), which has already been used for the deposition of corrosion protective films [20, 21] and is also known from adhesive bonding in automotive industry [22]. The deposition of silicon oxide films from a mixture of hexamethyldisiloxane and oxygen by using a dielectric barrier discharge (DBD) was studied to improve corrosive behaviour of steel [23].

Within the last years, deposition of plasma polymerized films by the DBD sources has been studied as well [24-28].

Atmospheric-pressure plasmas overcome the disadvantages of vacuum operation. It is a unique, non-thermal, glow-discharge plasma operating at atmospheric pressure. The discharge uses a high-flow feed gas consisting primarily of an air or N_2,also sometimes a small amount of O_2, H_2O or CF_4 can be introduced to generate reactive species [29]. This technique is environmentally benign and does not produce any liquid waste, which makes it also desirable for manufacturing. It has been shown to provide very high deposition rates. Additionally, no wet chemicals are involved, the thermal budget is low, and irregularly shaped surfaces can be coated with specially designed deposition parameters. In contrast to direct PECVD, a directional film deposition is obtained which effectively reduces the parasitic coating of the walls. Hence, frequent time-consuming and expensive reactor cleaning steps are avoided. Because of these advantages, the APCVD process is particularly attractive for the cost-effective fabrication of AR coatings. In the following, a comprehensive experimental study of the growth of porous SiO_2 and porous TiO_2 films by APCVD are presented. In order to fabricate porous SiO_2 films featuring very low refractive indices, the process parameters of a commercially available APCVD system were optimised like coating thickness, porosity etc. Low refractive index films are ideally suited for AR coatings.

2. EXPERIMENTAL PART

2.1 Materials and Surface Preparation

A hexamethyldisiloxane (HMDSO, $C_6H_{18}OSi_2$, Mol.Wt: 162.38, density: 0.764 g/mL at 20 °C (lit.), purity: 98.5%) and tetraisopropyl orthotitanate (TTIP, $C_{12}H_{28}O_4Ti$, Mol.Wt: 284.22, density: 0.96 g/mL at 20 °C(lit.), purity: 97%) were purchased from Sigma Aldrich, France, and were used in this study without further purification. For this study we had taken polished silicon wafers (100) purchased from Siltronix, France which were ultrasonically cleaned in acetone bath for 30 min and rinsed with ethanol for 30 min. Cleaned wafers were air dried and then used for FESEM and AFM analyses.

Field emission scanning electron microscopy (FESEM) images were taken using Zeiss Ultra 55 FEGSEM with GEMINI Column on gold metalized coating surfaces by sputter coating (Cressinton sputter coater-108 auto) in order to investigate the microstructure of the porous SiO_2 and TiO_2 films. The bulk morphology and thickness of the coatings were investigated by fracturing coatings deposited on Si wafers and then taking cross-sectional images of fractured samples. Electrons with accelerating voltage of 6 kV were used to obtain the FESEM images.

The average surface roughness (Ra) values were derived from (10 μm × 10 μm) AFM images. AFM imaging was performed in contact mode with gold coated "Scientific Instruments" V-shaped cantilevers (spring constant between 0.1 and 0.02 N/m). The images were treated with Gwyddion software. All of the AFM images were acquired at room temperature (~ 24 °C), in air and are presented as unfiltered data.

The bulk chemical environment of coatings was analyzed by a Fourier transform infrared spectrometer (Bruker-Tensor 27 FT-IR spectrophotometer) in the ATR mode. Silicon wafers (i-type, 100) were used as deposition

substrates for FT-IR analysis. The FT-IR spectra were recorded with the resolution of 4 cm^{-1} and averaged over 100 scans. All the FTIR spectra shown here were corrected for a sloping baseline.

2.2 Experimental Set up

For thin film deposition, we modified a plasma jet system from Plasmatreat GmbH was used [20-22,30]. A schematic of the plasma jet system modified for thin film deposition at open air is shown in Fig. 1. The Atmospheric Pressure Plasma Jet (APPJ) was operated with dry air at a flow rate of 1.3 to 43 standard liters per minute (slm). The center electrode was driven by an excitation frequency between 19 and 23 kHz, with a pulse peak power of approximately 900 to 1000 W. The PT400 generator delivers a pulse-pause modulated current. The current modulation is controlled by adjusting the plasma cycle time (PCT). With a PCT of 100 %, the pulse duration is equal to the pause duration. In fact, the generator is based on a patented impulse discharge double resonance system with pulse-pause modulation. When the PCT is equal to 100 %, the "on" time is equal to the "off" time, and this corresponds to a duty cycle of 50 %. To feed liquid or gaseous precursors into the plasma the precursor inlet was arranged at the nozzle exit of the plasma jet. The inlet was at the transition zone between the plasma excitation volume and the relaxing afterglow plasma. Plasma deposition was carried out with a venturi nozzle, which is moved over the surface with different displacement speeds and raster offset at a distance of 5-10 mm.

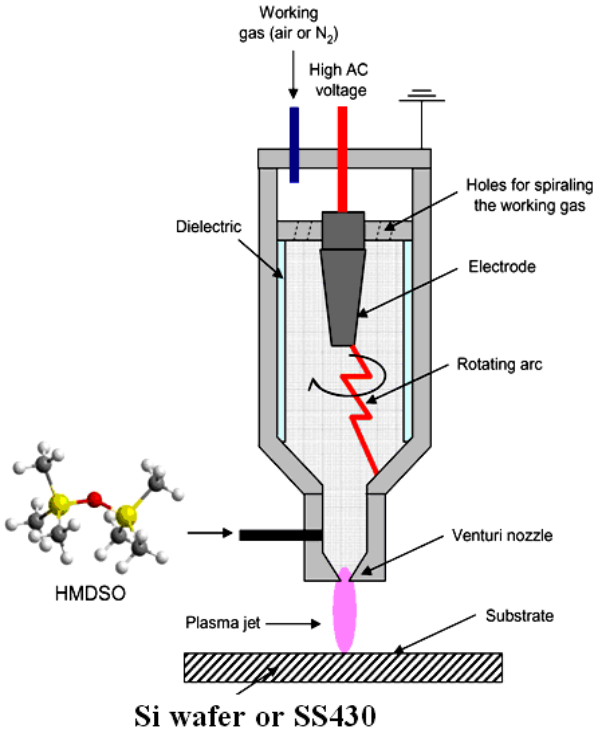

Fig. 1 *– Schematic of APCVD system with HMDSO precursor inlet*

In the case of HMDSO, we used the Plasmatreat GmbH system which is designed for deposition and where the precursor is vaporized in the evaporator and then introduced in the plasma jet. The discharge was used in pulsed mode with different PCT. The light emitted by plasma jet was monitored using Ocean Optics HR4000 spectrometer covering range 330-790 nm with resolution of 0.14 nm. The double mask in the front of optical fiber entrance was applied to obtain the space resolution better than 0.5 mm.

All spectra were recorded using 10 s total integration time to obtain good signal/noise ratios also for weaker lines and bands. The lines/bands with signal/noise ratios better than 10 were used for the further analyses. Spectral response of the optical setup was determined using Oriel standard calibrating lamp.NIST Atomic Spectra Database [31] and molecular spectra tables [32] were used for the spectra identification. The spectral constants from NIST[31] were used for the electron temperature calculations,constants given by Gilmore et al. [33] were used for the vibrational temperature calculation using molecular nitrogen spectra.

3. OPTICAL DIAGNOSTICS OF PLASMA

The optical emission spectra were used for the monitoring of all deposition processes. A typical example of spectra obtained in air and in air with HMDSO precursor is shown in Fig. 2 where the main spectral transitions are marked. Based on these measurements, the shape of plasma jet as well as some of it's properties were characterized.

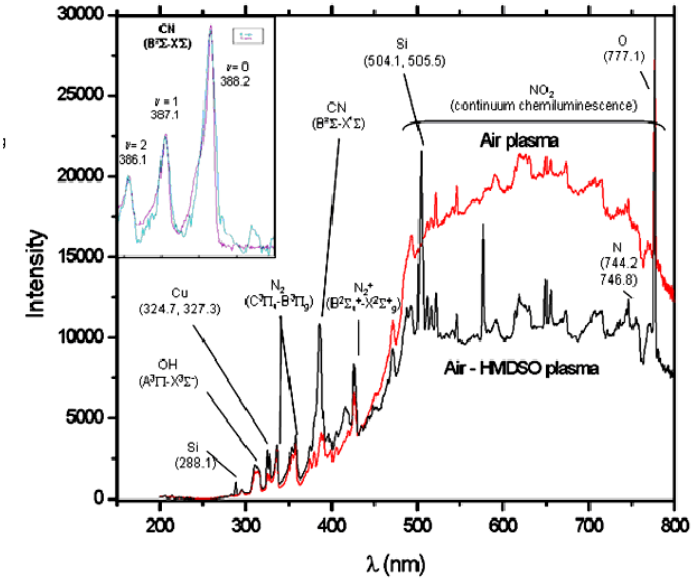

Fig. 2 – APPJ plasma diagnostic in air and air with HMDSO

3.1 Electron & Vibrational Temperatures of APPJ in Dry Air

The first part of the presented results shows the properties of APPJ generated in the dry air without any precursor at 1 kW power and 100 % PCT. It can be clearly seen that the discharge is nearly symmetric with some

turbulences at its edge as it is demonstrated in Fig. 3a for the atomic oxygen lines. The same profiles has been obtained also for the other particles identified in the spectra, i.e. atomic and molecular nitrogen and lines of chromium and copper introduced in the plasma due to the electrode erosion. To characterize the plasma itself, the electron temperature (in eV) was calculated using the intensities of 15 chromium lines. Also, 2D mapping was done for the axial and radial distribution of electron temperature (in eV) is shown in Fig. 3b. The vibrational temperature was calculated using nitrogen second positive bands of -2 sequence.

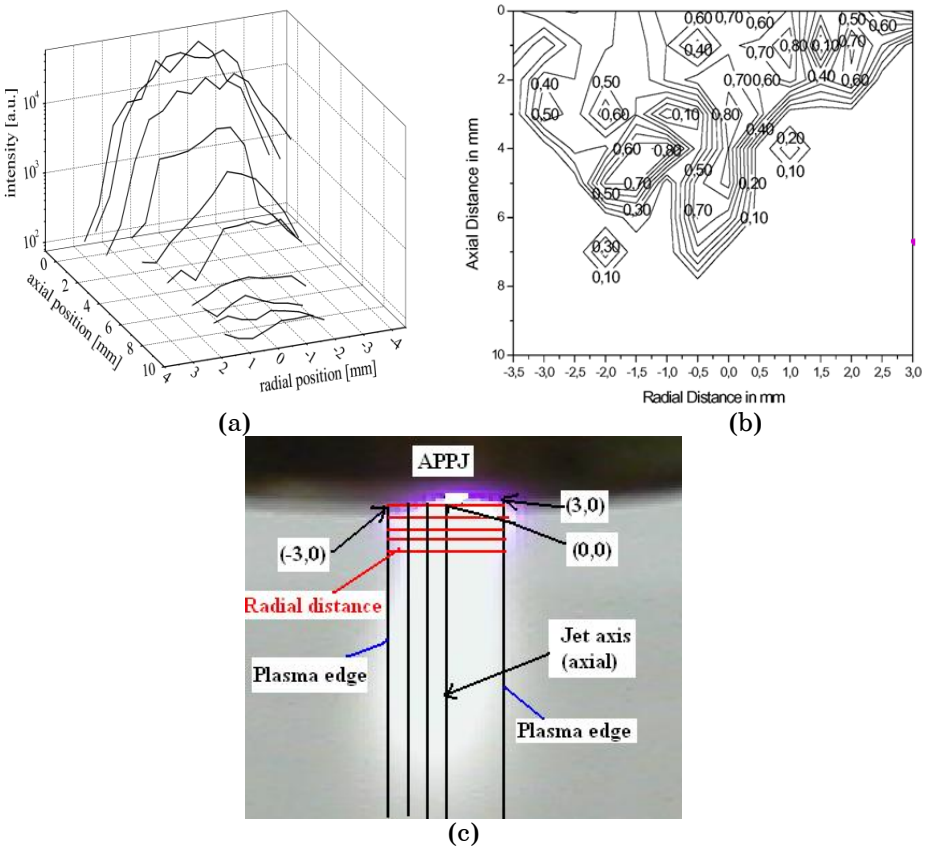

Fig. 3 *– The line profile of APPJ for spatially resolved intensity of oxygen at 777.194 nm (a) and 2D mapping of APPJ in dry air for the distribution of electron temperature (Te) in eV (b). APPJ mapping positions (c)*

Electron temperature was more or less linearly increased along the jet axis and it is determinable within 15 % uncertainty up to the distance of 5 mm form the nozzle. The radial profile of the electron temperature was very flat (not shown); the temperature at the plasma edge (Fig. 4c) was about 0.04 eV higher than that determined at the jet axis (Fig. 4a). Vibrational temperature of about 0.3 eV (with uncertainty again of about 15 %) was calculated which was nearly independent of the discharge position (Fig. 4b).

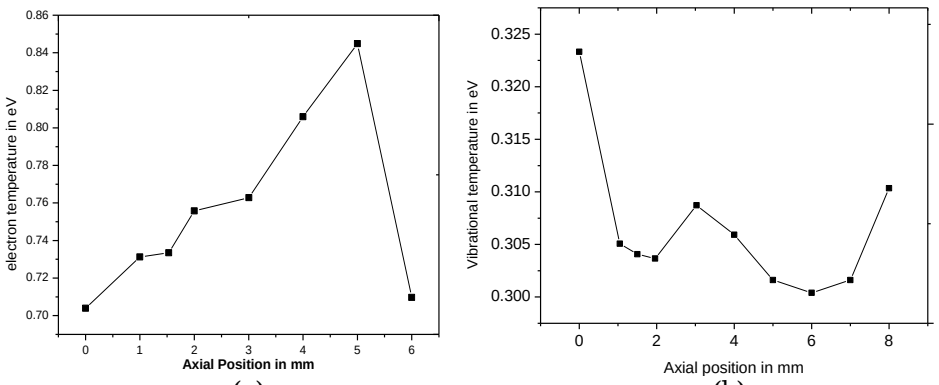

(a) (b)

Fig. 4 *– Electron (a) and vibrational temperatures of APPJ in dry air (b) at the jet axis*

3.2 Electron & Vibrational Temperatures of APPJ in Dry Air With Different HMDSO Monomer Flow Rates

Both temperatures were determined as a function of the axial position for different monomer flow rates at the same dry air mass flow as above. There is no significant change of the electron temperature value, but no temperature elevation with increase of the axial position was determined and thus the temperature is nearly constant at about 0.73 eV (Fig. 5a). Vibrational temperature determined from nitrogen second positive system is about 0.04 eV higher than in the plasma without monomer but it is nearly independent of the monomer flow rate (Fig. 5b). The temperature increase at larger distances from the nozzle is probably due to some energy transfer reactions in the decaying plasma.

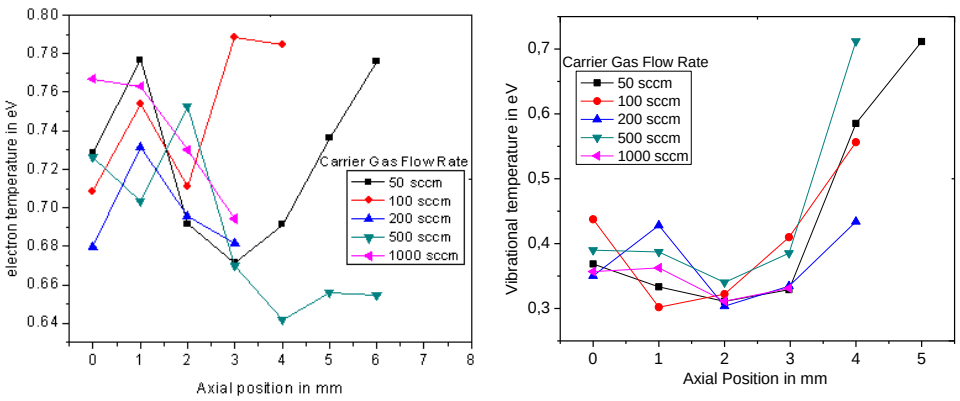

(a) (b)

Fig.5 *– Electron (a) and vibrational temperatures of APPJ in dry air with different HMDSO carrier gas flow rates (in sccm)*

The intensities of all of the excited species mentioned above as well as of atomic hydrogen and CN radicals show the similar profiles in the APPJ as it was presented in Fig. 2 for atomic oxygen. The increase of the intensity

with the enhancement of the monomer flow rate was observed for the species resulting from the fragmentation of the precursor and their reaction with the plasma gas such as H, CN etc but the others were more or less independent of the monomer mass flow rate.

3.3 Oxygen Line Intensity and at Different Plasma Cycle time (PCT)

The carrier gas flow rate was kept constant at 500 sccm at the applied power of 1 kW for these observations. As it can be seen, plasma generated at small PCT below 50 % was nearly non-radiating and thus also the temperature was not determined. At the higher PCT values, more or less no dependence on the PCT parameter was obtained (Fig. 6a and b). The discharge shape was nearly independent of the PCT however its dimensions (both axial and radial) increased with the increase of the PCT.

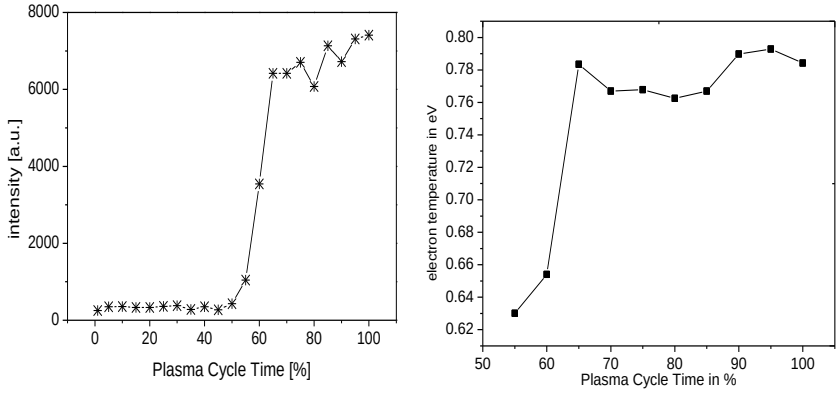

(a) (b)

Fig. 6 *– Intensity of oxygen line at* 777.194 *nm (a) and electron temperature of APPJ in dry air with* 500 *sccm of HMDSO monomer contained carrier gas flow as a function of plasma cycle time (PCT)*

4. ELECTRONE DENSITY MEASUREMENT OF APPJ

A single turn magnetic induction (B-dot) probe was used to measure B_r *(residual flux density)* inside the plasma volume. The B-dot probe consisted of a thin 50 ohms coaxial cable. A loop in the inner conductor of 0.3 cm diameter was made and connected to the outer conductor to complete the circuit. In uniform magnetic field, a time varying magnetic field $B(t)$ induces a voltage in a coil. The probe consists of a loop of wire which when subjected to a time varying magnetic flux obey Faraday's law. The latter is true when the cross sectional area of the coil is small enough so that the magnetic field does not vary over the area of the loop [34-36]. Circular Helmholtz coil was developed for magnetic field probe calibration [37] is shown in Fig. 7a. It allowed to obtain a uniformity of +/− 8% in the magnetic field in a volume of $5mm^3$ (Fig. 7b). The electron density was calculated around 10^{16} m^{-3} in dry air APPJ at 1kW power and 100 % PCT.

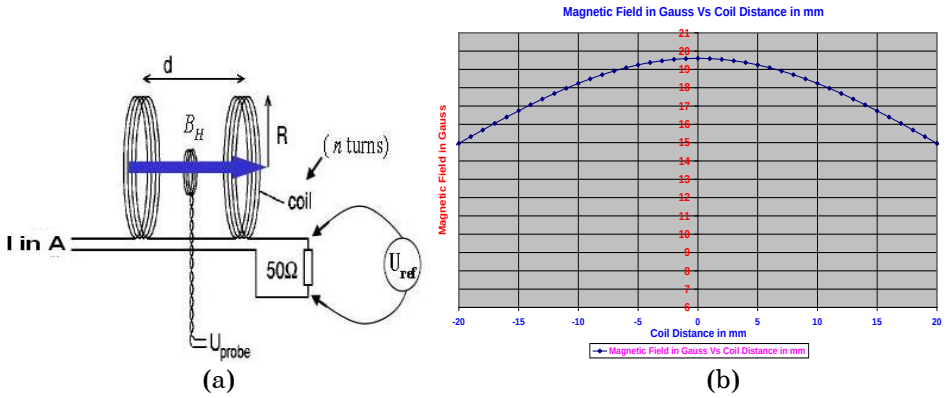

(a) (b)

Fig. 7 *– Schematic of circular Helmholtz coil arrangement (a) and magnetic field uniformity measurement (b)*

5. PLASMA GAS & MEASURE OF THE SUBSTRATE TEMPERATURE

Plasma gas was measured by using a K type thermocouple at different axial positions from the nozzle at different power conditions. A large temperature gradient was observed along the axis. As the distance from the nozzle increased, the temperature was decreased. Furthermore the increase of the PCT leads to an increase of the gas temperature (Fig. 8a).

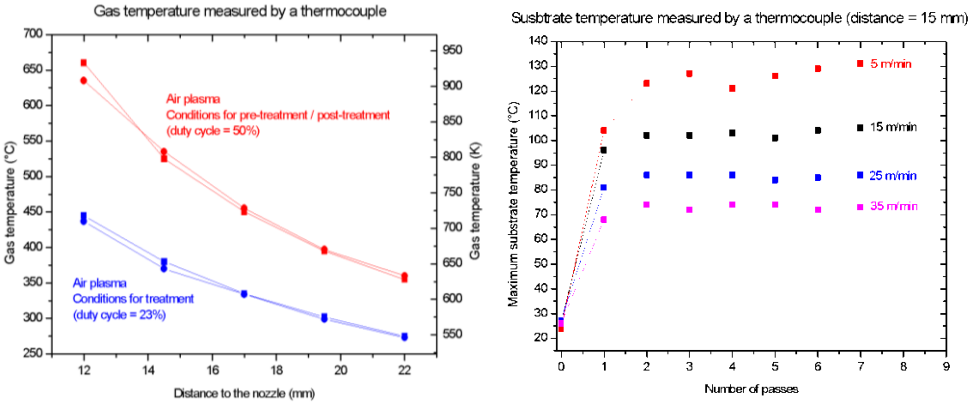

(a) (b)

Fig. 8 *– Gas temperature (a) and substrate temperature measurement by the thermocouple (b)*

The substrate temperature was measured by another K type thermocouple placed at 15 mm away from the nozzle at different jet displacement speeds and number of passes (Fig. 8b). It was observed very clearly that the temperature rise of the substrate depended on the jet speed and that it which leveled off after a maximum of 2 passes. Pretreatment on the substrate was performed at 450 °C and treatments at 350 °C.

6. RESULTS AND DISCUSSION

6.1 Preparation and Characterization of SiO_2 Films

Surface morphology of the coatings was analyzed by scanning electron microscopy and cross-section of a smooth & porous SiO_2 films (Fig. 9). It can be clearly seen that the structure of the layer is tightly dependent on the deposition conditions. Very smooth (R_a = 2.04 nm; R_q = 2.74 nm) and compact SiO_x layers can be created using the moderate concentration of precursor around 20 g/h (Fig. 9a). As monomer flow rate increase up to 40g/h, powder formation was observed (Fig.9b). Also, the cross section of the smooth SiOx film is shown in Fig. 9c.

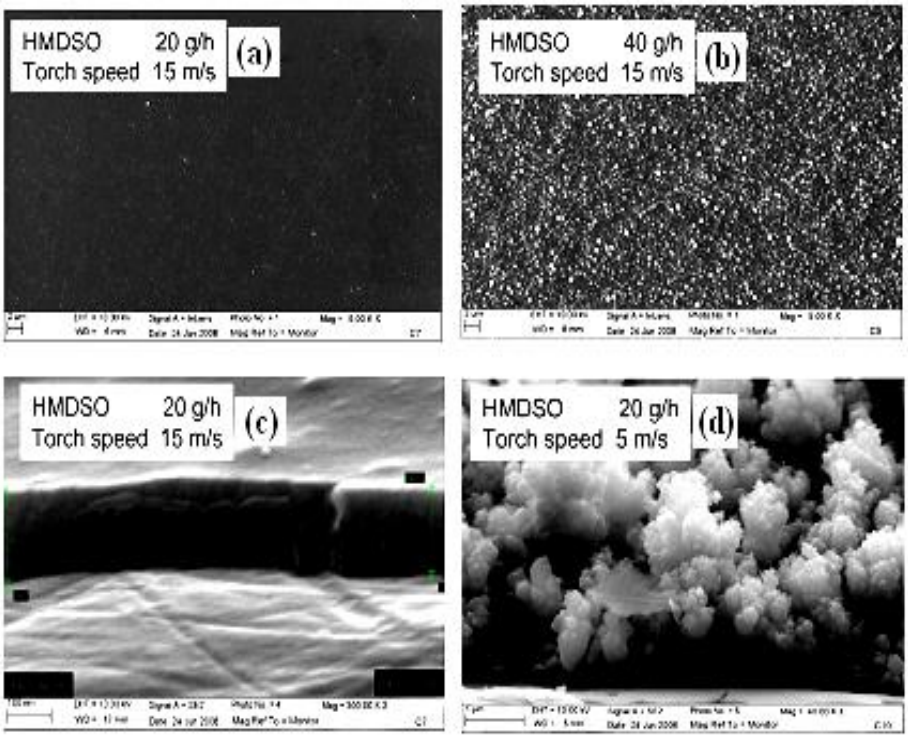

***Fig. 9** – FESEM images of smooth and porous* SiO_2 *films were deposited at different conditions (scale units of the upper images are* 2 *μm (a and b),* 100 *nm for the left bottom image (c) and 1 μm for the right bottom image (d))*

On the other hand, if low plasma jet speed is applied, the coating structure has an opened dendrite like structure with a very high specific area surface. Similar structures have been deposited in the case of titanium oxide which should have a great application potential mainly in deposition of photoactive titanium dioxide based thin layers. The deposition rate of these films was very high and it was typically of 800-1000 $nm.s^{-1}$ for the uniform films and over 3000 $nm.s^{-1}$ for porous layers. Porous SiO_x film was achieved at comparatively low jet speed 5m/min and 20gm/h HMDSO monomer feed ratio (Fig. 9d).

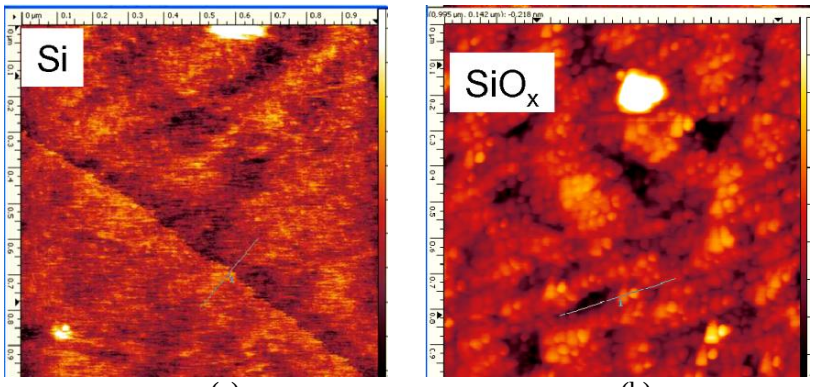

Fig. 10 *– AFM analysis of uncoated Si wafer, R_a = 0.106 nm, R_q = 0.175 nm (a), SiO_x film deposited at 920 nm/s on Si wafer, R_a = 2.04 nm, R_q = 2.74 nm (b).*

AFM result shows that it is possible to obtain very smooth SiO_x film (R_a = 2.04 nm, R_q = 2.74 nm) by APPJ even at high deposition rates 920 nm/s (Fig. 10b). Unfortunately, in the case of very rough films, it was not possible to define a thickness.

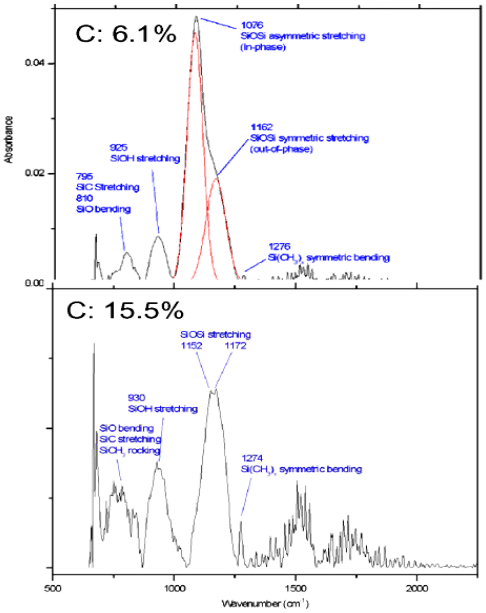

Fig. 11 *– FTIR spectra of plasma deposited SiOx coatings*

FT-IR spectra of plasma deposited porous SiO_2 coatings show that a dominating OSiO at 1070 cm^{-1} is observed throughout the whole foot print. The shift from 1000 cm^{-1} to 1070 cm^{-1} indicates an increase of the SiO_x stoichiometry. The longitudinal optical (LO) at 1200 cm^{-1}and the transverse optical (TO) modes of OSiO at 1130 cm^{-1} are a symptom of altered porosity

and compressive stress of the films and occur only in the periphery of the footprint. Moreover, the bending vibration of SiO at 808 cm^{-1} along with stretching vibrations of SiOH (930 cm^{-1}) and OH (3300 cm^{-1}) are present in the spectrum. The latter two are caused by water contaminations and hydroxyl groups. Depending on the experimental conditions and in particularly the flow rate of the HMDSO precursor, the deposited layers can be rich in carbon or which show a small amount of carbon (6 %) refers to Fig. 11.

6.2 Preparation and Characterization of TiO_2 Films

The preparation of TiO_2 films involves controlled monomer flow rate of TTIP in the APPJ nozzle at the given applied power and jet speed. The titanium precursor, being very hygroscopic and in order to avoid blocking the systems was fed into the plasma by usage of a bubbler at a constant temperature of 100 °C with pure N_2 as a carrier gas at a flow rate from 10 to 1000 standard cubic centimeters per minute (sccm). The discharge was created in the air or in N_2 at flow rate of 2400 l/hr. The deposition rate was up to 1 micron per second. OES measurement was performed in dry air plasma and also with TTIP precursor.

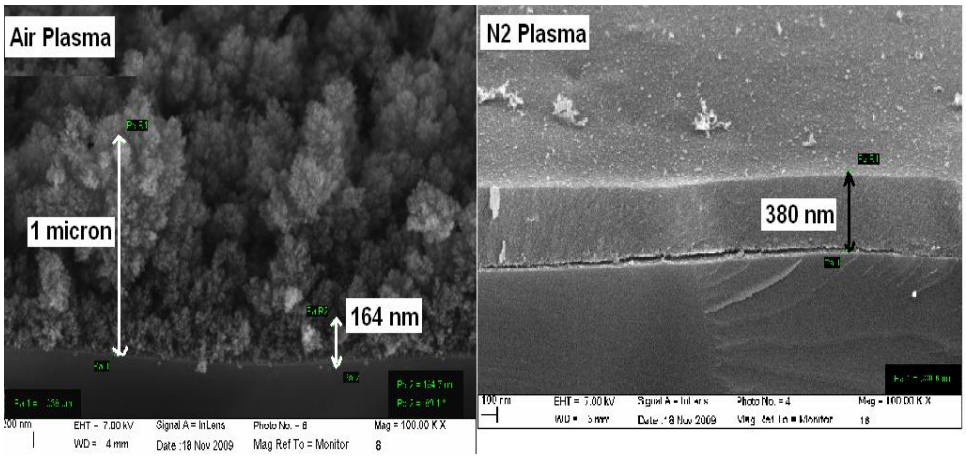

(a) (b)

***Fig. 12** – SEM images of plasma deposited TiO_2 coatings developed in air plasma (a) and N_2 plasma (b)*

It can be clearly seen that the layer structure tightly dependent on the deposition conditions. Porous and compact TiO_2 layers were obtained in air plasma and N_2 plasma at 1 kW power respectively. Plasma jet speed was 10m/min and N_2 was used as a carrier gas with the flow rate of 1000 sccm, which contained TTIP precursor vapour (Fig. 12). The deposition rate was around 1000 nm/sec in air plasma and 500 nm/s in N_2 plasma respectively at a same jet speed and precursor flow rate. The coatings deposited in N_2 plasma was much richer in carbon content as compared to ones deposited in the air (results not shown).

7. CONCLUSION

Smooth and porous SiO_2 is obtained by varying the deposition conditions which is useful for the AR coating in the PV module. Porous TiO_2 is also achieved by using the cost effective and environmental friendly APCVD technique. It was observed that electron temperature is independent of the monomer flow rate and PCT. The substrate temperature is very low in comparison to plasma and gas temperature. We observed high deposition rate and low carbon content in coatings deposited by APPJ. The as deposited films were amorphous, however after annealing in the air at 400°C, a mixture of anatase and rutile was observed. Also, the amount of anatase to rutile was improved by the annealing process.

Finally, APCVD is a cost effective, environmentally friendly and fast deposition technique which can be used to form AR coatings and DSSC solar cells on wide areas by using an array of plasma torches. This technique can be used to fabricate both AR coatings for solar cells but also for their passivation by the same process by varying the plasma condition.

We would like to thank Dr. C. Buske, Dr. A. Knospe and S. Gruber from Plasmatreat (Steinhagen, Germany) for their advices, technical and financial support. The authors thank also Dr. J. Polesel (CEA-Saclay, France) for AFM analysis.

REFERENCES

1. L.T. Canham, *Appl. Phys. Lett.* **57**, 1046 (1990).
2. Y.S. Tsuo, Y. Xiao, C.A. Moore, Z.C. Feng, R. Tsu, editors, 347, World Scientific Publishing Co., Singapore, (1994).
3. P. Menna and Y.S. Tsuo, L. Canham, editor, 384, INSPEC, The Institute of Electrical Engineers, London, (1997).
4. J. Zettner, H.V. Campe, M. Thoenissen, R. Auer, J. Ackermann, Th. Hierl, R. Brendel, M. Schulz, *2nd World Conf. on PV Solar Energy Conversion*, 1766 (1998).
5. L. Kore, G. Bosman, *Sol. Energ. Mat. Sol. C.* **57**, 31 (1999).
6. I.M. Thomas, *Appl. Opt.* **31**, 6145 (1992).
7. C.J. Brinker, G.W. Scherer, *Sol-Gel Science*, (Academic, New York, pp. 97, 228:1990).
8. L.M. Cook, K.H. Mader, *Opti. Eng.* **21**, SR-008 (1982).
9. K.W. Wecht, *Appl. Opt.* **30**, 4133 (1991).
10. H. Sakata, K. Aikawa, *J. Mater. Sci.* **19**, 2671 (1984).
11. P.G. Pal, S. Chao, G. Lucovsky, *J. Vac. Sci. Technol. A*, **4**, 689 (1986).
12. Y. Katayama, E. Ando, T. Kawaguchi, *J. Non-Cryst. Solids* **147**, 437 (1992).
13. A. Hagfeldt, M. Gratzel, *Acc. Chem. Re.* **33**, 269 (2000).
14. M. Gratzel, B.O`Regan, *Nature* **353**, 737 (1991).
15. U. Diebold, *Surf. Sci. Rep.* **48**, 53 (2003).
16. H.S. Chen, C. Su, C.K. Lin, Y.F. Hsieh, C.K. Yang, W.R. Li, *J. Chem. Eng. Jpn.* **42**, 36 (2009).
17. U. Lommatzsch, J. Ihde, *Plasma Process. Polym.* **6**, 642 (2009).
18. S.E. Babayan, J.Y. Jeong, A. Schutze, V.J. Tu, M. Moravej, G.S. Selwyn, R.F. Hicks, *Plasma Sources Sci. German Technol.* **10**, 573.(2001).
19. V. Hopfe, D. Rogler, G. Maeder, I. Dani, K. Landes, E. Theophile, M. Dzulko, C. Rohrer, C. Reichhold, *Chem. Vap. Deposition* **11**, 510 (2005)
20. EP1230414 P. Fornsel, C. Buske, U. Hartmann, A. Baalmann, G. Ellinghorst, K. Vissing. (2002).
21. R. Wilken, Neuss 20./21.03.2007.

22. German Published Patent Application, DE 102004033728A1.
23. C. Petit-Etienne, M. Tatoulian, I. Mabille, E. Sutter, F. Arefi-Khonsari, *Plasma Process. Polym.* **4,** S562 (2007).
24. R. Agostino, P. Favia, C. Oehr, M.R. Wertheimer, *Plasma Proc. Polym.* **2,** 7 (2005).
25. S. Paulusssen, R. Rego, O. Goossens, D. Vangeneugden, K. Rose, *J. Phys. D: Appl. Phys.* **38,** 568 (2005).
26. C.P. Klages, M. Eichler, R. Thyen, *New Diamond Front. Carbon Technol.* **13,** 175 (2003).
27. A. Sonnenfeld, T.M. Tun, L. Zajickova, K.V. Kozlov, H.E. Wagner, J.F. Behnke, R. Hippler, *Plasma Polym.* **6,** 237 (2001)
28. K. Schmidt-Szalowski, Z. Rzanek-Boroch, J. Sentek, Z. Rymuza, Z. Kusznierewicz, M. Misiak, *Plasmas Polym.* **5,** 173.(2000)
29. Z. Gao, J. Sun, S. Peng, L. Yao, Y. Qiu, *Appl. Surf. Sci.* **256,** 1496 (2009).
30. Ger. 29919142 (2001).
31. Yu. Ralchenko, A.E. Kramida, J. Reader, NIST ASD Team (2010).
32. R.W.B. Pearse, A.G. Gaydon, London, (1976).
33. F.R. Gilmore, R.R. Laher, P.J. Espy, *J. Phys. Chem. Ref. Data* **21,** 1005 (1992).
34. R. Piajak, V. Godyak, B. Alexandrovich, *J. Appl. Phys.* **81,** 3416 (1997).
35. R. Piajak, V. Godyak, B. 2Alexandrovich, *Rev. Sci. Instrum.* **72,** 4002 (2001).
36. H. Bhuyan, S.R. Mohanty, N.K. Neog, S. Bujarbarua, R.K. Rout, *Mess. Sci. Technol.* **14,** 1769 (2003).
37. C.M. Franck. O. Grulke, T. Klinger, *Rev. Sci. Instrum.* **73,** 3768 (2002).